J. Chem. Sci. (2019) 131:124
https://doi.org/10.1007/s12039-019-1705-7

REGULAR ARTICLE

Special Issue on 150 years of the Periodic Table

In silico design of pseudo D_{5h} actinide based molecular magnets: role of covalency in magnetic anisotropy

SOURAV DEY and GOPALAN RAJARAMAN*
Department of Chemistry, Indian Institute of Technology Bombay, Powai, Mumbai 400 076, Maharashtra, India
E-mail: rajaraman@chem.iitb.ac.in

MS received 20 July 2019; revised 25 October 2019; accepted 25 October 2019; published online 6 December 2019

Abstract. Actinide molecular magnets are of great interest in the area molecular magnetism as they possess strong covalency and spin-orbit coupling that their 4f congeners lack. Despite these known advantages, the actinide based molecular magnets have not been explored in detail due to the limited availability of actinide salts. While theoretical tools are proven to be useful in lanthanide chemistry towards prediction, they are still at an infant stage in actinide chemistry. In this manuscript, we have attempted to utilise CASSCF/RASSI-SO calculations to predict suitable pseudo D_{5h} molecules possessing attractive magnetic properties. To begin with, we have undertaken an extensive benchmarking of the methodology employed by studying two sets of isostructural, $[NdTp_3]$, $[UTp_3]$, $[Nd(COT'')_2]^-$, $[U(COT'')_2]^-$ {Tp^- = trispyrazolylborate, COT'' = bis(trimethylsilyl)cyclooctatetraenyl dianion} complexes. The method assessment reveals that the methodology employed is reliable as this has reproduced the experimental observables. With this, we have moved forward with prediction where pseudo-D_{5h} symmetric $[L_2M(H_2O)_5][I]_3L_2.(H_2O)$ {M = Nd, U, Pu; L = ^{t}BuPO(NH^{i}Pr)$_2$} systems are modelled from their Nd(III) X-ray structure. Our calculations reveal that the Uranium complex studied possess superior SIM characteristics compared to its lanthanide analogue. Plutonium complex has prolate electron density at the ground state, and hence the ligand environment is unsuitable for yielding SIM behaviour. The role of solvent molecules, counter anions and equatorial and axial ligand are explored and tantalizing prediction with a barrier height of 1403.3 and 989.5 cm^{-1} are obtained for $[^t$BuPO(NH^{i}Pr)$_2$-U-^{t}BuPO(NH^{i}Pr)$_2]^{3+}$ and $[Pu(H_2O)_5]^{3+}$ models, respectively and this paves the way for synthetic chemist to target such geometries in actinide based SIMs.

Keywords. Single-ion magnets; actinide magnets; magnetic anisotropy; CASSCF; QTM; U_{eff}.

1. Introduction

Molecular magnetism is one of the growing areas of interest because of its proposed potential application in information storage devices as it reduces the length scale.[1–5] A groundbreaking advancement has been made in this area very recently where the blocking temperature (T_B) below which the magnetisation is considered frozen enhanced up to liquid nitrogen temperatures, and this has drawn the attention of chemists to design potential single-molecule magnets (SIMs).[6,7] Enhancing the T_B beyond the liquid helium temperatures is essential for any futuristic applications. The blocking temperature in a way is correlated to the barrier height for magnetisation reversal (U_{eff}), though the terms that are binding these two factors are not known at present. The U_{eff} is defined as the effective barrier below which the magnetisation relaxes spontaneously, and this is often derived assuming Orbach/other relaxation processes. Two factors control the U_{eff} values of Lanthanide based SIMs: (i) the energy splitting between the ligand field separated states and (ii) the magnitude of ground state m_J level.[8–10] In the recent past, an effort has been put forward to increase the ligand field strength to enhance the energy gap between the ground state m_J components in lanthanide-based systems.[11–15] Since the 4f orbitals are deeply buried, it feebly

*For correspondence

Electronic supplementary material: The online version of this article (https://doi.org/10.1007/s12039-019-1705-7) contains supplementary material, which is available to authorized users.

interacts with the ligands leading to small crystal field splitting among the ground state m_J components. Depending on the nature of the electron density of the Ln(III) ion, one can design ligand that can yield a substantial barrier for magnetisation reversal. For example, Dy(III) possessing oblate electron density when $m_J = 15/2$ is stabilised requires strong axial ligation to yield large U_{eff} values. Over the years, various ligand design has been proposed to enhance the axiality of the Dy(III) ion based SIMs. Several Dy(III) SIMs are reported recently to possess substantial U_{eff} values, and in some cases, the so-called "axial limit" where the splitting of the $^6H_{15/2}$ state of Dy(III) nearly equals to Spin-Orbit coupling is already reached and hence provide a bottleneck to enhance the U_{eff} further.[6,7]

One possible way to go beyond the axial limit is to increase the interaction of 4f orbitals with ligands, and this is very challenging given the fact that these orbitals are inert and do not have radial nodes to offer strong mixing with the ligand orbitals. An alternative idea to enhance the axiality is to use congeners of lanthanides, i.e., actinides. In actinides, the 5f orbitals strongly interact with ligands, thanks to the presence of radial nodes and diffuse nature of the 5f orbitals, it mixing with the ligands are often compared to that of the 3d transition elements. This has sparked attention in the actinide based SIMs in recent years with many uranium and post-uranium based SIMs reported with attractive blocking temperatures.[16–22]

Over and above the application that are proposed for actinide based SIMs, they are also potential targets for nuclear fuel reprocessing and can activate small and inert molecules such as CO_2, N_2 and H_2.[10,17,18,21–31] The 5f orbital of actinide displays strong spin-orbit coupling and the SOC constant values of the actinides are of the order of 10^3 cm^{-1} and this is nearly an order of magnitude higher compared to that of the lanthanides (10^2 cm^{-1} for lanthanides).[32] However, there are significant challenges in actinide chemistry: unlike lanthanide chemistry which has been pursued wieldy in various laboratories, synthesis of actinide complexes face severe restriction all around the world, and only a handful laboratory across the globe have access and are working in the actinide based SIMs. This severely restricts the trial-and-error method of synthesising the compounds that exist in lanthanides that offer an extensive database of compounds to study and understand its magnetic characteristics. Thus, only a handful of actinide SIMs are reported to date.[18,21–24,29,31]

Computational methods based on multireference CASSCF calculations have proved to be an indispensable tool in lanthanide chemistry for not only understanding the ground-state electron density but also to derive the qualitative mechanism for magnetisation relaxation. These methods are so robust that they are utilised to make predictions, and several such predictions have already seen the daylight, offering confidence in the methodology employed.[33,34] In actinide chemistry as well, the computational tools can offer a remedy where one can utilise the well-established computational protocol to predict target structures that are expected to exhibit desired magnetic characteristics.

Among various geometries that are proven to be successful in Lanthanide chemistry, pseudo D_{5h} geometry stand tall for the following reasons: (i) this geometry offers a very large blocking temperature for the Dy(III) SIMs, (ii) these ligand architecture are the only one that offer air-stable magnets at present as desired for any potential applications, (iii) they offer a unique opportunity for chemist to attempt to make the structural analogues by replacing the lanthanide metals with other metal salts, and (iv) by designing various equatorial ligands, already a large set of D_{5h} Dy(III) SIMs are reported that are well-characterised using both experiments and theory.[12,14,35,36] Here we attempt to combine the above two points, i.e., using the robust computational methods to model potential actinide SIMs and utilize the pseudo D_{5h} symmetry geometries that are known for Lanthanides as a starting point for this prediction with an aim to design and develop *in silico* actinide SIMs possessing attractive magnetic properties.

Though the aforementioned methods have been thoroughly tested by us and others for lanthanide chemistry, it is important to benchmark the methods for actinide compounds using reported complexes and magnetic data.[11,14,17,35,37–39] Hence, here our aims are two-fold: (i) to assess the methodology for isostructural lanthanide and actinide complexes to gain confidence on the methodology employed and (ii) utilise these established methodologies to predict the magnetic properties of actinide D_{5h} molecules. Henceforth, here we have studied two isostructural lanthanide and actinide analogues (i) $[NdTp_3]$ (**1**) and $[UTp_3]$ (**2**) (Tp^- = trispyrazolylborate), (ii) $[Nd(COT'')_2]^-$ (**3**) and $[U(COT'')_2]^-$ (**4**) (COT″ = bis(trimethylsilyl)cyclooctatetraenyl dianion) that are reported in the literature and its magnetic properties established.[29,30] Both the molecules are characterised as SIMs albeit with a barrier height of 2.84 and 3.81 cm^{-1} for complexes **1** and **2** respectively. Similarly, complexes **3** and **4** is also found to exhibit slow relaxation of magnetisation with an U_{eff} value of 14.6 and 18.8 cm^{-1}, respectively.

Secondly, our group in collaboration with Murugavel and co-workers studied pseudo D_{5h} symmetric

$[L_2Nd(H_2O)_5][I]_3L_2.(H_2O)$ (L = $^tBuPO(NH^iPr)_2$) (**5**) which is reported to have a blocking barrier (U_{eff}) of 27.2 cm^{-1} – the highest among Nd(III) SIMs.[39] Here we have modelled actinide complexes based on the geometry of complex **5**, whereby Nd is replaced by uranium and plutonium leading to $[L_2U(H_2O)_5][I]_3L_2$ (**6**) $[L_2Pu(H_2O)_5][I]_3L_2$ (**7**). Further, in order to grasp various structural features that could influence the barrier height we have assessed (i) solvent molecules present on the crystal lattice, (ii) counter anion that are present in the periphery of the metal ion, (iii) role of equatorial ligands on the barrier height, and (iv) role of axial ligands in the U_{eff} values using various models that are constructed from the structures of complexes **5**–**7**. Our study offers significant insight into the D_{5h} actinide SIMs, posing potential target molecules that could be attempted in the years to come.

2. Results and Discussion

2.1 *Benchmarking the methodology by computing magnetic anisotropy of complexes 1–4*

In this section, we will compare the two sets of isostructural lanthanide and actinide analogues (i) $NdTp_3$ (**1**) and UTp_3 (**2**) (ii) $[Nd(COT'')_2]^-$ (**3**) and $[U(COT'')_2]^-$ (**4**). **1** and **2** are reported to have U_{eff} of 2.84 and 3.81 cm^{-1} respectively in the presence of an external magnetic field.[29] *Ab initio* study on both complexes reveals large transverse anisotropy in the ground state (Tables S1 and S2, SI). The energy gap between the ground and first excited Kramers doublets (KDs) is estimated to be 87.5 and 251.5 cm^{-1} for $NdTp_3$ and UTp_3, respectively. The energy splitting of the KDs generated from ground state m_J reaches up to 269.7 and 943.9 cm^{-1} for Nd and U respectively which implies that the interaction between metal and ligand is ionic in the former while it is covalent in the latter case (Figure 1, S1 and Tables S1, S2, SI).

The computed spin-orbit coupling turns out to be larger compared to the crystal field splitting, and this indicates that m_J is a good quantum number for actinides in +3 oxidation state (Figure 2). The magnetic susceptibility of both complexes computed using the minimal active space agrees well with experiment and infers the reliability of our approach (Figure 3). The magnetic susceptibility of **1** is higher compared to that of **2** at all temperatures due to small crystal field splitting of the former (which allows it the access all the KDs generated from the ground state m_J). The ground state is dominated by $m_J = |\pm 5/2>$ along with a minor contribution from $|\pm 7/2>$ state which is similar for the trigonal prismatic geometry studied by our group earlier (Figure 1c and 1d).[27] The α-electron density of ground state m_J reveals dominant oblate shape in case of uranium (Figure S2, SI). Using the computed wavefunction, the ligand field parameters were derived using Steven formalism $H_{CF} = \sum \sum_{k=-q}^{q} B_K^q \tilde{O}_k^q$ where $B_k^q$and $\tilde{O}_k^q$ are the computed crystal field (CF) parameters and Stevens operator respectively.[40,41] The crystal field parameter of uranium has been calculated considering lanthanide analogue (Nd).

The B_2^0 crystal field parameter is more significant in **2** compared to **1** and suggests that the QTM will be smaller in **2** compared to complex **1** (see Table S3, SI). Although the thermally-assisted QTM (TA-QTM) is small, the complexes will relax *via* first excited state due to non-coincidence of the g_{zz} anisotropy axis between the ground and first excited state for **2** and very small transition probability to first excited state in **1** (Figure 1, Tables S1–S2, SI). The mismatch of the energy gap between the ground and first excited KDs with the experimental blocking barrier is correlated with the large QTM which will render the molecule to relax *via* the first excited state. In our earlier study, the $6d_z^2$ orbital was found to be lower in energy in trigonal prismatic geometry, and hence the addition of this orbital in the active space improved the result dramatically.[27] Since the geometry of complex **2** is also trigonal prismatic, we have performed additional calculations including $6d_z^2$ orbital in the active space. The computed magnetic susceptibility with this setup is found to be closer to the experimental one compared to the minimal reference space utilized and this is in agreement with our earlier results. The addition of $6d_z^2$ orbital also lowers the energy of the computed KDs (Table S4, SI). The $6d_z^2$ orbital in the trigonal prismatic environment plays an important role in magnetic anisotropy.

For complexes $[Nd(COT'')_2]^-$ (**3**) and $[U(COT'')_2]^-$ (**4**), the U_{eff} is reported to be 14.6 and 18.8 cm^{-1}, respectively.[30] This U_{eff} is larger compare to complexes **1–2,** and this is due to higher symmetry present in complexes **3–4**. The anisotropy axis in these complexes is found to orient along the C_2 axis (Figure 4a and 4b). The computed g tensors expose small transverse anisotropy in the ground state, which leads to smaller QTM in the ground state (Tables S5 and S6 (SI) and Figure 4c, 4d). Although the transverse anisotropy is small in the first excited state, the molecule is expected to relax via this state due to non-coincidence of the g_{zz} anisotropy axes between the ground and first excited state (Tables S5 and S6, SI). The energy gap between the ground and the first excited

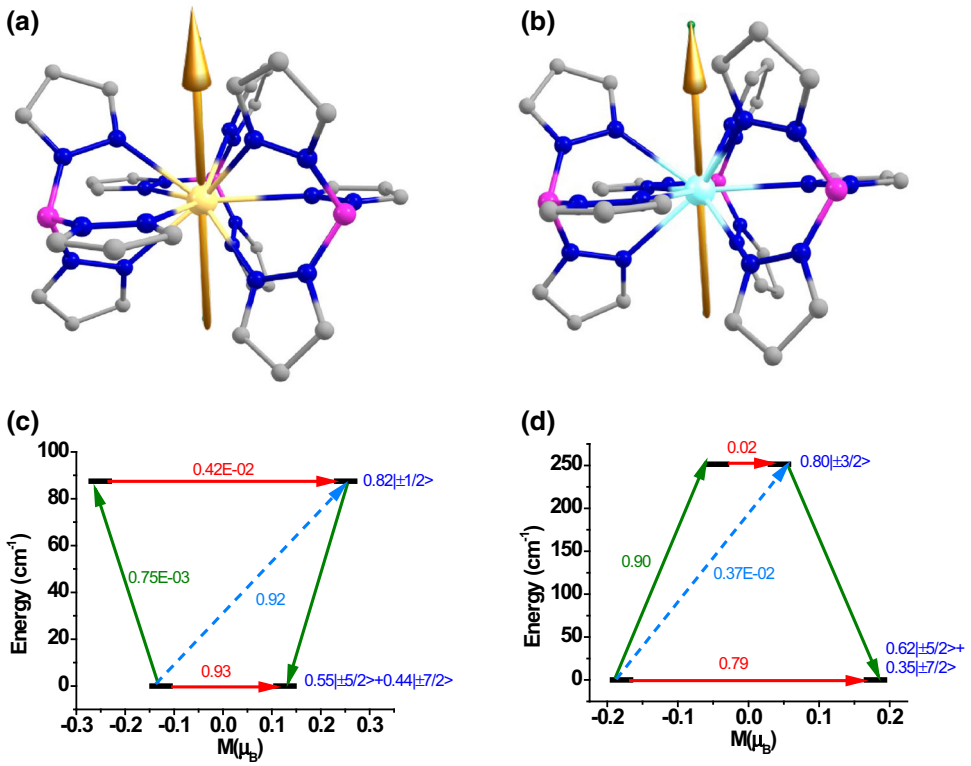

Figure 1. (a) The anisotropy axis of **1**. (b) The anisotropy axis of **2**. Hydrogens are omitted for clarity. Colour code: Nd-yellow, U-cyan, N-blue, C-grey, B-pink. (c) The mechanism of magnetic relaxation of **1**. (d) The mechanism of magnetic relaxation of **2**. The red line represents QTM *via* ground states and TA-OTM *via* excited states. The dashed sky blue line indicates possible Orbach process. The olive line indicates possible pathways of magnetic relaxation. The blue characters indicate the m_J composition of the Kramers doublet (KD) derived from the $^4I_{9/2}$ ground state.

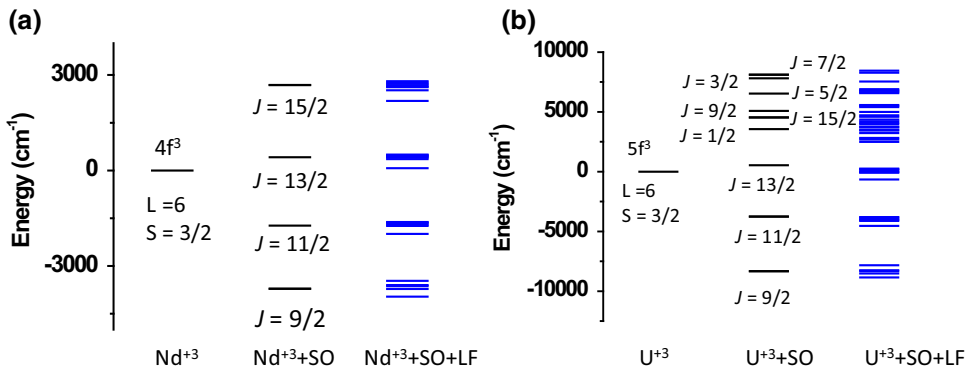

Figure 2. (a) Scalar relativistic ^4I energy level for an isolated Nd^{3+} ion (left) split by RASSI-SO into *J*-multiplet structure (centre). The *J*-multiplets are further split by the ligand field (LF) of in **1**. (b) Scalar relativistic ^4I energy level for an isolated U^{3+} ion (left) split by RASSI-SO into *J*-multiplet structure (centre). The *J*-multiplets are further split by the ligand field (LF) of in **2**.

KDs is estimated to be 207.4 and 382.0 cm^{-1} (calculated barrier height for magnetisation reversal; U_{cal}) which is significantly overestimated compared to the experimental blocking barrier (Tables S5 and S6, SI). The energy splitting of the ground state KDs reach up to 627.8 and 1554.2 cm^{-1} for **3** and **4** respectively denotes larger covalency in η^8-U-COT bond compare to η^8-Nd-COT bond. The magnetic susceptibility of both complexes computed is in good agreement with the experiments offering confidence on the employed methodology (Figure 5). Again the magnetic susceptibility of the **3** is higher compared to **4** due to smaller crystal field splitting of the former (which allows it the access all the KDs generated from the ground state m_J in lanthanides). The computed spin-orbit coupling becomes larger compare to crystal field splitting

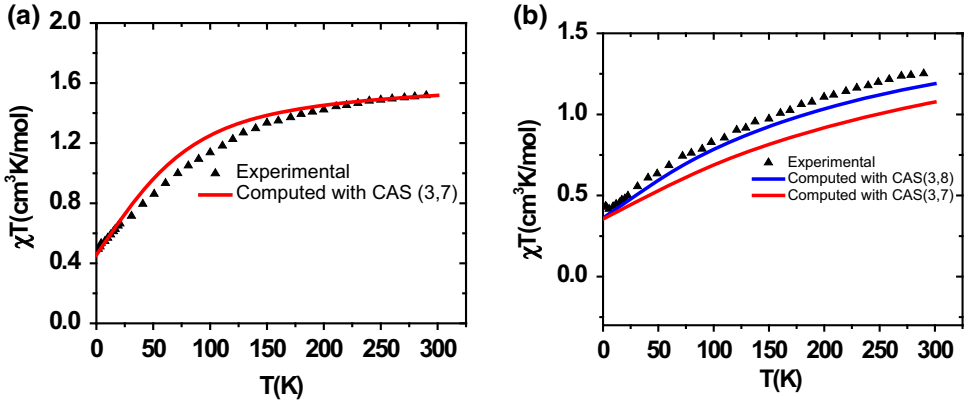

Figure 3. (a) Comparison of experimental and computed magnetic susceptibility of **1**. (b) Comparison of experimental and computed magnetic susceptibility of **2**. *Ab initio* data has been scaled to 0.93 for **1** to reproduce the experimental values.

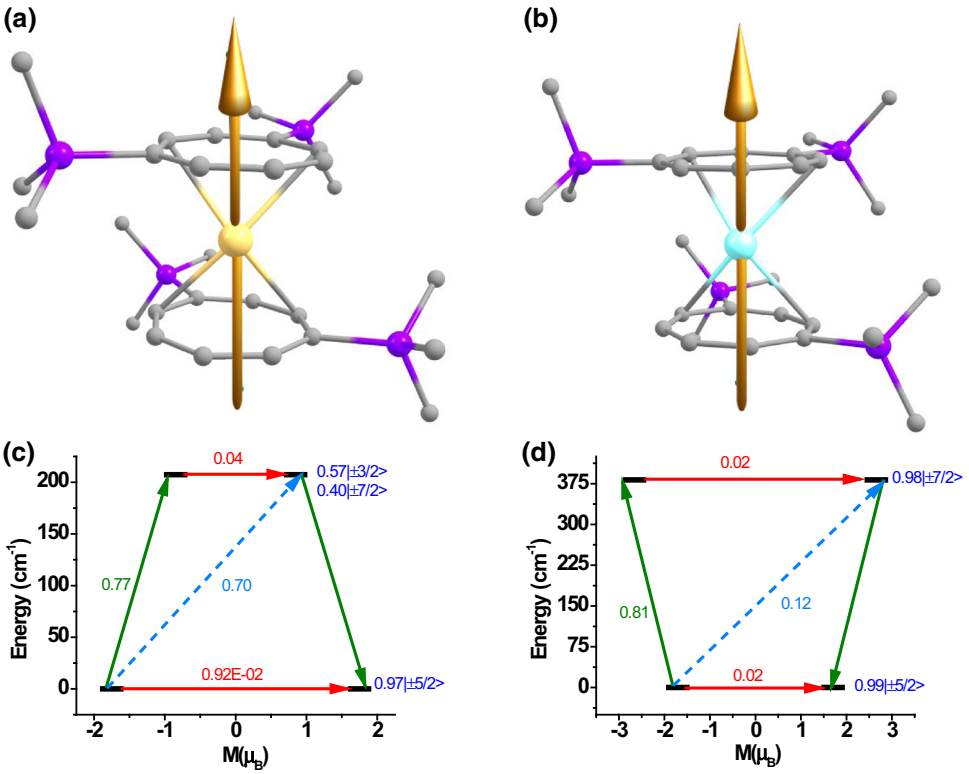

Figure 4. (a) The anisotropy axis of **3**. (b) The anisotropy axis of **4**. Hydrogens are omitted for clarity. Colour code: Nd-yellow, U-cyan, C-grey, Si-purple. (c) The mechanism of magnetic relaxation of **3**. (d) The mechanism of magnetic relaxation of **4**. The red line represents QTM *via* ground states and TA-OTM *via* excited states. The dashed sky blue line indicates possible Orbach process. The olive line indicates possible pathways of magnetic relaxation. The blue characters indicate the m_J composition of the Kramers doublet (KD) derived from $^4I_{9/2}$ ground state.

denotes that m_J is a good quantum number for actinides in +3 oxidation state (Figure S3, SI). The ground state is conquered by m_J = |±5/2> which renders the molecule to relax *via* first excited state (Figure 4c and 4d). This is one of the key causes for the large difference between the U_{eff} and U_{cal} values. (See Figure S4 (SI) for oblate electron density of complexes **3** and **4**). The energy splitting of the KDs generated from m_J = |±9/2> is more than two times larger in **4** compared to **3** which implies that Nd-ligand bond is less covalent compare to U-ligand bond (see Figure S5 in SI). The computed crystal field parameter shows larger B_2^0 value in neodymium analogue but the B_2^1 and B_2^{-1} are comparable to B_2^0 whereas, B_2^1 and B_2^{-1} are smaller than B_2^0 in uranium analogue (see Table S7, SI). This implies that the $[U(COT'')_2]^-$ is strongly axial in nature compare to $[Nd(COT'')_2]^-$.

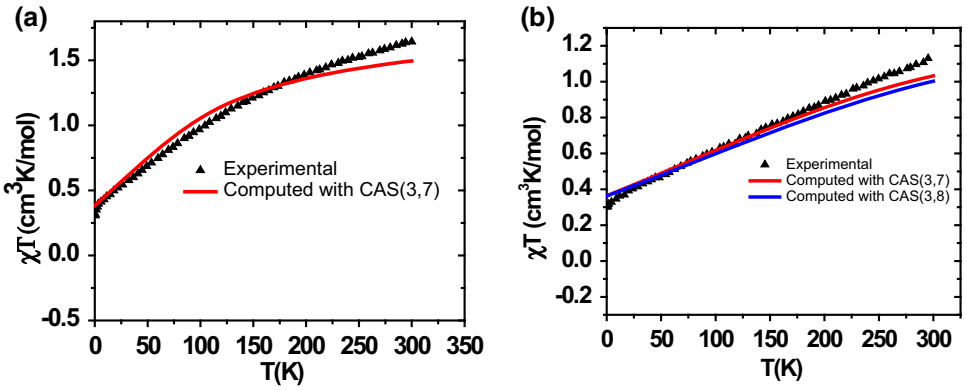

Figure 5. (a) Comparison of experimental and computed magnetic susceptibility of **3** (b) Comparison of experimental and computed magnetic susceptibility of **4**. *Ab initio* data has been scaled to 1.09 for **3** to reproduce the experimental values.

In complex **4**, the $6d_z^2$ was not found to be lower in energy. Therefore, the computed results using CAS (3,8) does not provide any better agreement compared to CAS(3,7) reference space (Table S8 (SI) and Figure 5b). Therefore in the next section, we have used the CAS (3,7) methodology for our calculations.

2.2 *In silico design of U(III) and Pu(III) D_{5h} SIMs*

By studying complexes **1–4**, it is clear that Uranium(III) has an oblate electron density (if the ground state m_J stabilised is $|\pm 9/2>$). In this esteem, plenty of Dy complex with D_{5h} symmetry has been reported with large blocking barrier as well as blocking temperature when the axial ligands are strong donors compared to equatorial ones.[11,12] But there are only a handful of Nd complexes reported with SIM properties.[29,30,39,42–44] The Nd complex $[L_2Nd(H_2O)_5][I]_3$.L_2.(H_2O) (**5**) synthesized by Murugavel and coworkers exhibit the largest U_{eff} of 27.2 cm^{-1} among all D_{5h} symmetric Nd(III) SIMs known.[39] Here we have replaced the Nd(III) by U(III) to yield corresponding $[L_2U(H_2O)_5][I]_3L_2$ (**6**) complex. The geometry of this complex has been optimised using density functional methods to have realistic structural parameters (See computational details in SI). The optimised structure, along with selected structural parameters and the computed ground state g_{zz} axis for complex **6** is given in Figure 6 and S6 (SI). The equatorial U-O bond length infers the non-uniform distribution of bond lengths because of the non-equivalent hydrogen bonding interaction between equatorial hydrogen of water and Iodine and solvent molecules. The axial U-O bond length is shorter compared to the equatorial U-O bond length because of the strong donation of the phosphonic diamide axial ligand (Figure 6). As seen in Nd(III) and also in Dy(III) geometry, the equatorial water molecules are in H-bonding interaction with the lattice Iodine ions and this freeze the possible H-atom rotation. *Ab initio* multireference calculations have been performed on both **5** and **6** displays a very small transverse anisotropy in the ground state which clues to very small QTM (Figure 6c, 6d and Table 1). The anisotropy axis is oriented along the C_5 axis, i.e., along with the O-U-O bond (Figure S6, SI). The $m_J = |\pm 9/2>$ state becomes the ground state in both uranium and neodymium complexes (Figure 6c and 6d). So far, no complexes of U(III) have been reported with $m_J = |\pm 9/2>$ ground state (Figure 6). The energy gap between the ground and first excited KDs as well as overall crystal field splitting generated from ground state m_J becomes larger in uranium complexes compare to neodymium complexes (Table 1).

The qualitative mechanism of magnetisation relaxation developed reveals that both of these complexes will relax *via* first excited KDs due to the large transverse anisotropy (Figure 6c and 6d). The larger difference between the U_{eff} and U_{cal} value of **5** is due to the fact that the calculations have not taken into consideration intermolecular interactions and Raman relaxation mechanism. As seen earlier, the α- electron density plotted shows oblate shape in line with the magnetic properties computed (Figure 7a and 7b). The computed crystal field parameter implies the ligand field is axial in nature in both the complexes (Tables S9 and S10, SI).

The complexes **5** and **6** displays hydrogen bonding interaction with solvent molecules and counter anions. The ab initio study has been undertaken on the model systems of **5** and **6** to find the role played by the solvent molecules and counter anions (**5a** and **6a** where solvent molecules have been removed, **5b** and **6b** where counter anions also removed from **5a** and **6a**). The calculation on **5a** and **6a** reveals larger KD1-KD2 energy gap, as well as overall energy splitting of the

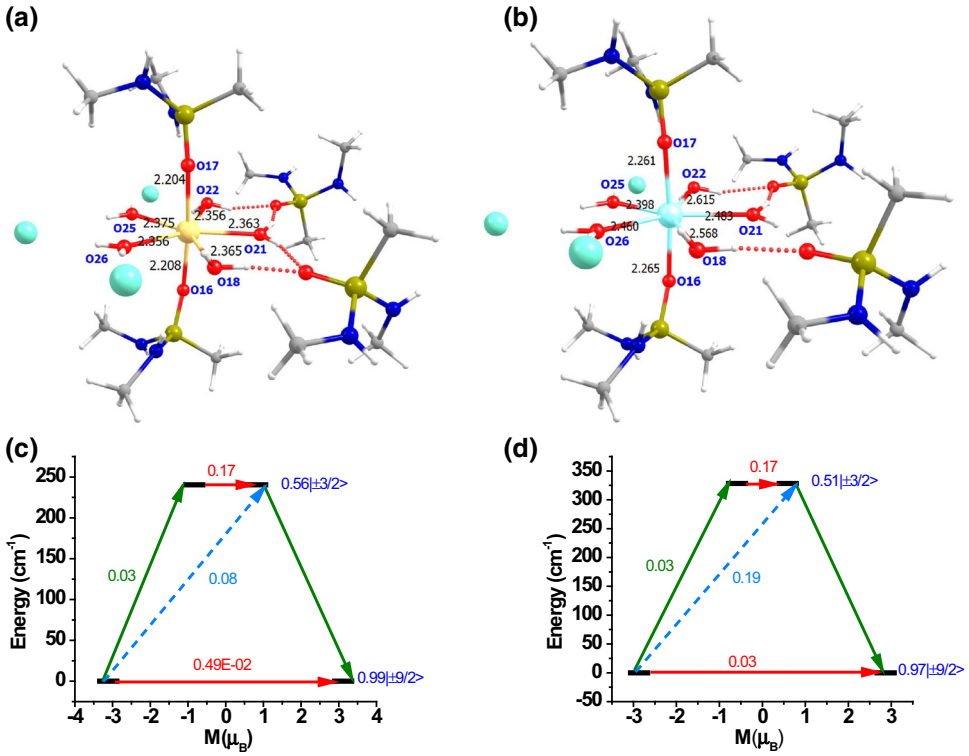

Figure 6. (a) X-ray structure of **5** showing the Nd-O bond lengths. (b) Complex **6** with U-O bond lengths. Colour code: Nd – yellow, U – cyan, I – deep cyan, N – blue, O – red, C – grey, P – greenish yellow, H – White. (c) The mechanism of magnetic relaxation of **5**. (d) The mechanism of magnetic relaxation of **6**. The red line represents QTM *via* ground states and TA-OTM *via* excited states. The dashed sky blue line indicates possible Orbach process. The olive line indicates possible pathways of magnetic relaxation. The blue characters indicate the m_J composition of the Kramers doublet (KD) derived from the $^4I_{9/2}$ ground state.

ground state m_J, compared to **5** and **6** (Table 1, Figures 8 and S7, SI). Since the solvent molecules are involved in hydrogen bonding interaction with equatorial water molecules, the removal of those molecules decreases the LoProp charge of equatorial water oxygens and thus increases the LoProp charge of axial ligand oxygens (Tables S11 and S12, SI). The increase of axiality is evident from the larger B_2^0 value in **5a** and **6a** compare to **5** and **6**, respectively (Tables S9 and S10, SI). Furthermore, a closer look at the α-electron density of ground state m_J reveals (Figures 9 and S8, SI) that the removal of solvent molecules increases the oblate nature of the electron density and this is due to lesser mixing of the ground state m_J levels with the higher excited state.

Secondly, to find out the role of counter anions in magnetic anisotropy, we have removed the counter anions from models **5a** and **6a** and carved out models **5b** and **6b** respectively. Calculations on these models reveal that the energy splitting between KD1 and KD2 increases and this is accompanied by a large decrease in transverse anisotropy (Table 1). These features are reflected in the qualitative mechanism of magnetic relaxation (Figures S9 and S10, SI) where QTM becomes significantly smaller, and one can expect a zero-field SIM for these models or the corresponding realist structures if made (Figures S7 and S8, SI). A closer look at the α electron density reveals that oblate nature enhances further in models **5b** and **6b** (Figures 9 and S8, SI). The LoProp charge indicates a decrease in the equatorial oxygen atom charges and an increase in the axial oxygen atoms charges for **5b** and **6b** as compared to **5a** and **6a**, respectively (Tables S11 and S12, SI). Again this is due alteration in the strength of hydrogen bonding, and hence this increases the axiality in these model further (Tables S8 and S9, SI).

Thirdly, we have carried out another set of *ab initio* calculations whereby models **5c** and **6c** are constructed by removing the equatorial water molecules in models **5b** and **6b**, respectively. The transverse anisotropy in the ground state KD decreases drastically in these models, and this is reflected in estimated negligible QTM value in the ground and first excited KDs (Table 1, Figures S9 and S10, SI). The energy splitting between KD1-KD2 as well as overall KDs splitting generated from the ground state m_J reaches the axial limit (Table 1, Figures 8, S7, SI). The non-coincidence of the anisotropy axis between the ground and

Table 1. CASSCF+RASSI-SO computed relative energies of the low lying KDs along with g tensors of **5**, **6** and **7** and the models derived from it.

Energy (cm^{-1})	g_x	g_y	g_z	Energy (cm^{-1})	g_x	g_y	g_z
		5				**6**	
0.0	0.013	0.016	6.231	0.0	0.080	0.106	5.737
240.4	0.033	0.704	5.168	328.3	0.107	0.325	4.759
330.7	0.005	0.711	5.239	518.2	0.515	1.175	4.153
367.6	0.732	1.396	4.058	601.1	0.311	1.209	3.918
497.4	0.461	0.527	5.034	1021.0	1.231	1.558	4.217
		5a				**6a**	
0.0	0.013	0.016	6.169	0.0	0.114	0.124	5.394
312.6	0.276	1.023	5.069	427.4	0.169	0.419	4.577
405.5	0.619	1.995	4.156	580.3	0.346	0.945	3.943
436.2	0.168	1.428	4.040	689.4	0.407	1.257	4.308
562.6	1.357	1.465	4.397	1209.1	2.066	2.169	3.128
		5b				**6b**	
0.0	0.004	0.007	6.227	0.0	0.011	0.018	5.857
448.6	0.380	1.239	4.965	605.2	0.122	1.485	4.293
516.3	3.930	2.791	0.908	796.4	1.246	1.470	4.223
575.0	0.276	0.797	4.061	867.2	0.293	0.603	4.536
634.3	0.101	0.313	4.762	1147.9	0.305	0.496	4.691
		5c				**6c**	
0.0	0.000	0.000	6.231	0.0	0.000	0.000	6.371
859.8	0.033	0.084	4.141	1403.3	0.005	0.050	3.967
967.0	0.384	0.540	1.996	1544.8	0.547	0.623	2.053
1031.9	0.034	0.043	5.431	1820.1	0.021	0.027	5.490
1220.3	4.181	3.157	0.463	1990.3	4.246	3.002	0.526
		5d				**6d**	
0.0	0.757	2.212	4.630	0.0	4.271	2.645	0.765
195.6	0.953	1.558	2.354	362.7	2.231	1.436	0.227
344.4	0.389	1.014	5.175	735.5	0.297	1.917	3.825
388.3	0.115	1.127	4.922	854.2	0.983	1.272	4.705
559.9	0.007	0.014	6.623	1199.4	0.023	0.046	6.444
		7				**7a**	
0.0	1.125	0.971	0.013	0.0	1.043	0.970	0.077
366.3	0.030	0.071	1.220	462.8	0.026	0.091	1.336
1155.9	0.046	0.087	2.613	1414.7	0.120	0.189	2.807
		7b				**7c**	
0.0	0.976	0.884	0.248	0.0	0.919	0.826	0.365
642.6	0.020	0.033	1.672	936.5	0.003	0.003	2.350
1899.9	0.000	0.107	3.353	2848.9	0.002	0.006	4.936
		7d					
0.0	0.025	0.046	1.205				
989.5	0.087	0.095	0.134				
1687.4	1.216	0.995	0.087				

first excited KDs will force the molecule to relax *via* the first excited state leading to the U_{cal} value of 859.8 and 1403.3 cm^{-1} for models **5c** and **6c**, respectively (Figures S9 and S10, SI). In these models, the m_J = |±9/2> becomes largely stabilised compared to other m_J levels signifying stronger axial interaction in the absence of any equatorial ligands. The α- electron density generated from the ground state m_J has pure oblate shape revealing negligible/no mixing of the ground state m_J with higher excited states (Figures 9 and S8, SI). This is also supported by the CF B_2^0 and LoProp charges (Tables S9–12, SI).

In the next step of calculations, we have decided to remove the axial phosphonic diamide ligand keeping only the equatorial water molecules intact to assess the role of equatorial ligation in controlling the magnetic anisotropy. For these, we have further carved out models **5d** and **6d** from their corresponding structures where only the five water molecules are kept and all other ligands/solvent/counter-anions are removed.

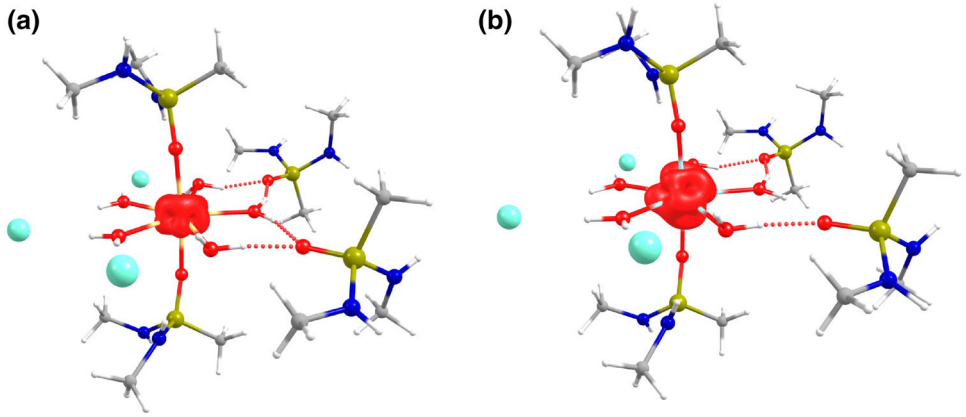

Figure 7. (a) Alpha electron density **5**. (b) Alpha electron density of **6**. Colour code: Nd – yellow, U – cyan, I – deep cyan, N – blue, O – red, C – grey, P – greenish yellow, H – White. The electron density surface shown corresponds to a value of 0.023 e^- per $bohr^3$.

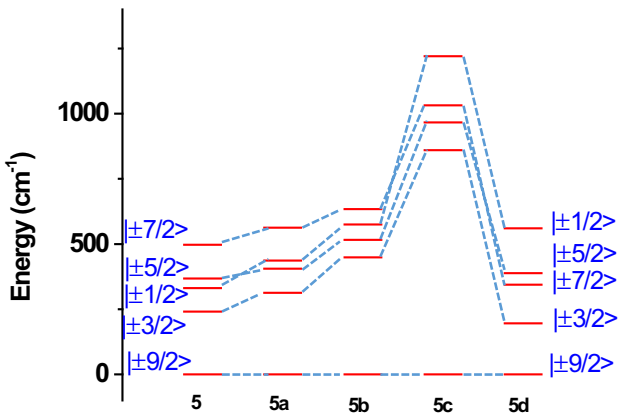

Figure 8. Evolution of m_J level energies of **5** and the models derived from it.

Calculations reveal a large transverse anisotropy in the ground state for these models, and the large ground state QTM values accompany this (Table 1, Figures S9 and S10, SI). The QTM becomes larger in **6d** compared to **5d** since uranium is more susceptible to the ligand field compared to the corresponding lanthanide. These models are predicted to relax *via* ground KDs itself, leading to the expectation of no SIM behaviour whatsoever in these cases. Both models have large easy plane anisotropy and with m_J = |±9/2> being the ground state in **5d** but m_J = |±1/2> being the ground state in **6d** (Figures 8 and S7, SI). This dramatic change in the ground state m_J again reflects a fact that actinide faces stronger electrostatic ligand interaction compared to the lanthanides. (Figure 8 and S7, SI). The energy splitting of the KDs generated from ground state m_J is still comparable to **a** and **b** models suggesting the ligand field generated from the water molecules is moderate (Figures 8 and S7, SI). The α electron density becomes prolate in **6d** (m_J = |±1/2> is ground state) but in **5d** has both prolate and oblate characters (m_J = |±9/2> is ground state with strong mixing with higher excited m_J states, Figures 9 and S8, SI). All these observations are also supported by the computed CF parameters and the LoProp charges (Tables S9–S12, SI).

To increase the covalency further, we have undertaken *ab initio* study on another optimised model complex $[L_2Pu(H_2O)_5][I]_3L_2$ (**7**) where Nd in **5** has been replaced Pu. The optimised bond length of Ac-O (Ac = actinide) decreases as we move right to the periodic table i.e., from U to Pu due to the increased covalency in the same order (Figures 6 and 10). The *ab initio* multireference calculations on complex **7** reveal large transverse anisotropy in the ground KD, which leads to very larger QTM in the ground state (Table 1 and Figure S11, SI). The anisotropy axis here is oriented along the C_2 axis, i.e., along with the O-Pu-O bond (Figure S12, SI). The very small ground state magnetic moment leads to the stabilisation of m_J = |±1/2> state (Figure S11, SI). Since the energy gap between the spin-orbit coupled state of Pu^{+3} ion is much larger than the ligand field separated spin-orbit coupled state, m_J is expected to be a good quantum number here (Figure S13, SI). The prolate shape for α electron density also implies that m_J = |±1/2> is the ground state (Figure 10). The larger covalency of Pu-O bond compare to U-O leads to the larger KD1-KD2 energy gap in the former (Table 1). The LoProp charge analysis also reveals a larger negative charge on axial oxygen atoms compared to equatorial oxygen atoms for complex **7** (Table S13, SI). As this ligand framework is unsuitable for prolate, one can expect that the corresponding Pu(III) molecule is unlikely to exhibit SIM behaviour.

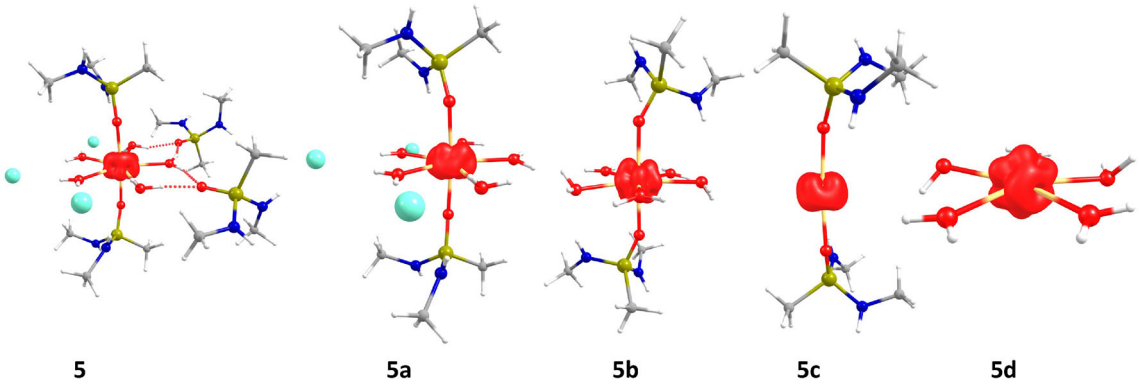

Figure 9. Alpha electron density of ground state m_J of **5** and the models derived from it. Colour code: Nd – yellow, I – aqua, O – red, N – blue, C – grey, P – greenish yellow, H – white. The electron density surface shown corresponds to a value of 0.023 e^- per $bohr^3$.

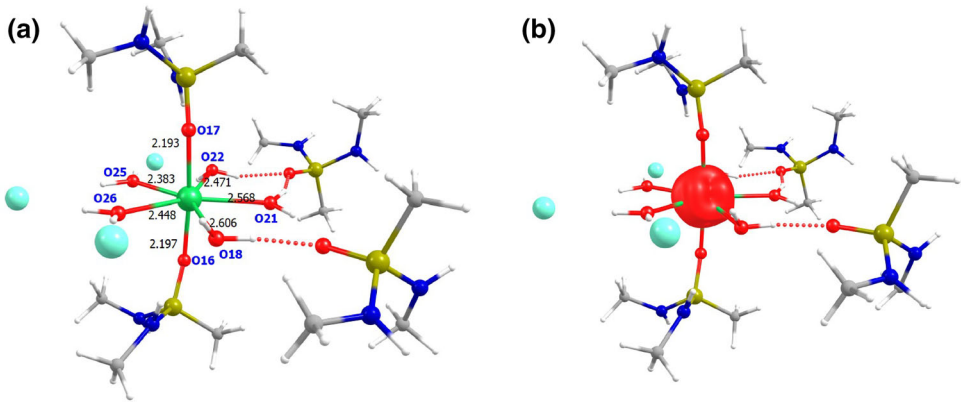

Figure 10. (a) Optimized structure of **7** with Pu-O bond length. Colour code: Pu-green, I-aqua, O-red, N-blue, C-grey, P-greenish yellow. (b) The alpha electron density of **7**. The electron density surface shown corresponds to a value of 0.023 e^- per $bohr^3$.

Further, just like in complex **6**, here as well, we have performed an in-depth analysis of the various factor that influences the barrier height. This has been carried out by performing calculations on a series of models constructed from the optimised structure of complex **7**. Removing the solvent molecules (**7a**) lead to lowering of LoProp charge in the equatorial oxygen atoms which in turn increases the prolate nature of the α electron density generated from the ground state m_J level (the $m_J = |\pm 1/2>$ becomes the ground state; Table S13, Figures 11, S14, SI). The lowering of LoProp charge in the equatorial oxygen atoms is comprehended from the disappearance of hydrogen bonding interaction between solvent oxygen and hydron atom of equatorial water molecules. The ground state is comprised of sizeable transverse anisotropy where g_x, $g_y >> g_z$ (Table 1) is due to the prolate nature of electron density. However, the energy gap between KD1-KD2 as well as overall energy splitting of the KDs generated from the ground state m_J increases in this model system (Figure S14, SI). The next set of models were constructed by removing counter anions (model 7**b**) and here the transverse anisotropy is found to be very large (Table 1) which is also supported by the $m_J = |\pm 1/2>$ ground state. The LoProp charge is found to further decrease in the equatorial oxygen atoms, and increases in the axial oxygen atoms (Table S13, SI). This charge distribution is suitable for the oblate type ions but not for Pu (Figure 11). The energy gap between the KD1-KD2 as well as the overall energy splitting of the ground state KDs increases due to the removal of counter anions (Table 1 and Figure S14, SI).

To test the Pu(III) at the axial limit, the equatorial water molecules have been removed from model 7**b** to carve out model **7c**. Here the energy gap between KD1-KD2, KD1-KD3 increases and reaches the axial limit (Figure S14, SI and Table 1). As expected, the LoProp charge on the coordinating oxygen atoms becomes very large compared to **7a-b** (Table S13, SI). The transverse anisotropy in the ground state also becomes very high (Table 1) and density also

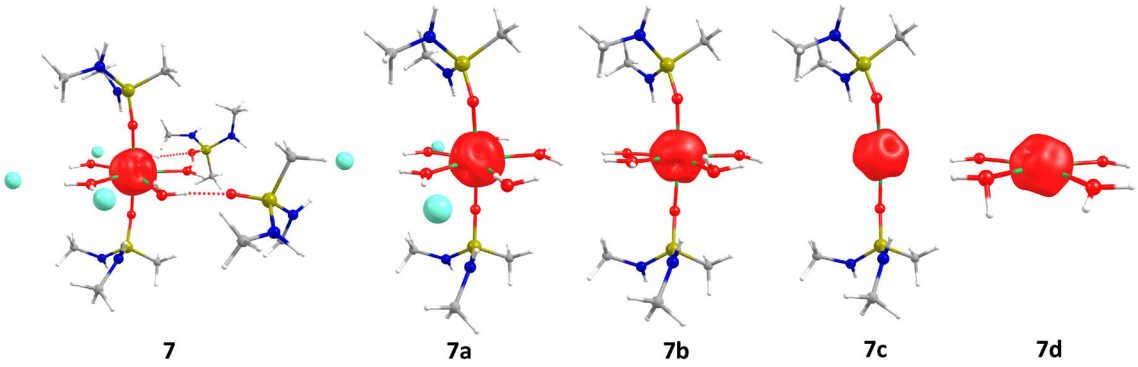

Figure 11. Alpha electron density of ground state m_J of **7** and its derivatives. Colour code: Pu-green, I-aqua, O-red, N-blue, C-grey, P-greenish yellow, H-white. The electron density surface shown corresponds to a value of 0.023 e^- per $bohr^3$.

resembles the shape of prolate reflecting why the computed parameters are not that great for this model (Figure 11).

Since the axial ligand field is not suitable for Pu to attain zero-field SIM properties *ab initio* calculation has been performed on model complex **7d** where axial ligands are removed from **7b**. In this model, only the equatorial water molecules are retained. The calculations reveal very small transverse anisotropy in the KD1 which is also reflected in the very small QTM value (Table 1 and Figure S11, SI). The $m_J = |\pm 5/2\rangle$ and $|\pm 3/2\rangle$ becomes the ground and first excited states, respectively with the non-coincidence of the anisotropy axis between the two which will force the molecule to relax *via* this excited state. This model complex is very promising and expected to possibly exhibit zero-field SIM with the estimated barrier U_{cal} value of 989.5 cm^{-1} (Table 1 and Figures S11, S14, SI). Clearly, with this ligand field, the α electron density of the ground state m_J becomes oblate in nature, and thus the explains the aptness of the ligand field present in this model (Figure 11). The axial crystal field parameter (B_2^0) becomes larger compared to the non-axial parameter as expected (Table S14 (SI), The crystal field parameter was calculated by replacing Pu with lanthanide analogue, i.e, Sm).

3. Conclusions

In this work, we have performed *ab initio* multireference calculations on various lanthanide and actinide complexes to gain insight into the nature of magnetic anisotropy in these systems. The conclusion derived from this work is summarised below:

(a) To begin with, we have performed method assessment for the suitability of the CASSCF/RASSI-SO/SINGLE_ANISO approach for actinide by computing various experimental observables such as g-tensors, magnetic susceptibility data and barrier height for magnetisation relaxation for isostructural lanthanide and actinide complexes. For this purpose, we have chosen four complexes name, $[NdTp_3]$, $[UTp_3]$, $[Nd(COT'')_2]^-$, $[U(COT'')_2]^-$. The methodology employed reasonably reproduces all the experimental parameters, though there is a significant deviation in the computed barrier height. Inclusion of $6d_z^2$ orbital in the reference space tends to improve the susceptibility, but not significantly, the U_{cal} values. However, actinides are not issued here, as shown earlier all the lighter lanthanide suffers from this issue and this is also clearly present in actinides. This could be associated with the prominence of non-Orbach relaxation processes, but this is not very clear at this stage.

(b) We have utilised the pseudo D_{5h} geometry that is known for Lanthanide to model corresponding uranium, and plutonium complexes and *ab initio* calculations have been undertaken in these structures. Clearly, the U(III) found to have significant interaction with the ligand with the overall crystal field is found to enhance two times larger compared to the corresponding Nd(III) structure. Similarly, Pu(III) also exhibits larger crystal field splitting and here the splitting is 2.3 times larger compared to Nd(III). Both this point reveal a long suspected but not quantified point that actinide tends to have stronger interactions with the ligand leading to greater anisotropy.

(c) The U(III) D_{5h} complex exhibits oblate electron density and hence found to yield reasonably good SIM characteristics. The enhancement of the U-Ligand covalency also has an adverse effect, as reflected in the increase in the QTM probability compared to the corresponding lanthanides. This is

primarily attributed to the fact that the five equatorial water molecules that are known to have the destructive effect on the barrier height on the lanthanide, just got worse in U(III). The Pu(III) on the other hand, has a prolate electron density and is thus clearly unsuitable for D_{5h} geometry as reflected in the substantial transverse anisotropy and QTM probabilities estimated.

(d) To improvise the predictions on actinide models, a series of calculations on model systems were performed whereby systematically the lattice solvents, counter-anions, equatorial water and axial phosphonic diamide ligands are removed. These models yield significant insight into the nature of anisotropy and how metal ions such as U(III) could potentially yield superior SIMs.

(e) Among all the models computed $[^{t}BuPO(NH^{i}Pr)_2\text{-}U\text{-}^{t}BuPO(NH^{i}Pr)_2]^{3+}$ and $[Pu(H_2O)_5]^{3+}$ found to yield extraordinary SIM characteristics with estimated U_{cal} value of 1403.3 and 989.5 cm^{-1}, respectively. These are some of the best numbers that are predicted for the actinide complexes. While we acknowledge that synthesis of such low-coordinate U(III) systems are going to be extremely challenging, our predictions reveal that if made, these molecules could possess very attractive magnetic properties and may even surpass the corresponding Lanthanide analogues.

To this end, we have utilised a combination of DFT methods and *ab initio* CASSCF calculations to predict suitable actinide molecules within the framework of pseudo D_{5h} symmetry to yield superior SIM characteristics. Our results yield some outstanding target molecules that are potentially ground-breaking within actinide based SIMs, if synthesised.

Supplementary Information (SI)

Supplementary Information consists of computational details, magnetic relaxation mechanism pathways, computed g tensor of the Kramers doublets, prolate/oblate electron density, the evolution of energy diagram with models, computed crystal field parameter, the direction of the anisotropy axis.

Acknowledgement

S. D. thanks UGC for SRF fellowship and CRAY supercomputing facility of IIT Bombay. GR would like to thank UGC (UGC-UKIERI Grant Number 184-1/2018(lC)) and SERB (CRG/2018/000430), CSIR (Sanction letter No. 01(2980)/19/EMR-II) for funding.

References

1. Sessoli R, Gatteschi D, Caneschi A and Novak M 1993 Magnetic bistability in a metal-ion cluster *Nature* **365** 141
2. Leuenberger M N and Loss D 2001 Quantum computing in molecular magnets *Nature* **410** 789
3. Bogani L and Wernsdorfer W 2010 In *Nanoscience and Technology: A Collection of Reviews from Nature Journals* (UK: Macmillan and Singapore: World Scientific) pp. 194–201
4. Christou G, Gatteschi D, Hendrickson D N and Sessoli R 2000 Single-molecule magnets *Mrs Bull.* **25** 66
5. Neese F and Pantazis D A 2011 What is not required to make a single molecule magnet *Faraday Disc.* **148** 229
6. GoodwinC A, Ortu F, Reta D, Chilton N F and Mills D P 2017 Molecular magnetic hysteresis at 60 kelvin in dysprosocenium *Nature* **548** 439
7. Guo F-S, Day B M, Chen Y-C, Tong M-L, Mansikkamäki A and Layfield R A 2018 Magnetic hysteresis up to 80 kelvin in a dysprosium metallocene single-molecule magnet *Science* **362** 1400
8. Woodruff D N, Winpenny R E and Layfield R A 2013 Lanthanide single-molecule magnets *Chem. Rev.* **113** 5110
9. Liddle S T and van Slageren J 2015 Improving f-element single molecule magnets *Chem. Soc. Rev.* **44** 6655
10. McAdams S G, Ariciu A-M, Kostopoulos A K, Walsh J P and Tuna F 2017 Molecular single-ion magnets based on lanthanides and actinides: Design considerations and new advances in the context of quantum technologies *Coord. Chem. Rev.* **346** 216
11. Gupta S K, Rajeshkumar T, Rajaraman G and Murugavel R 2016 An air-stable Dy(III) single-ion magnet with high anisotropy barrier and blocking temperature *Chem. Sci.* **7** 5181
12. Liu J, Chen Y-C, Liu J-L, Vieru V, Ungur L, Jia J-H, Chibotaru L F, Lan Y, Wernsdorfer W and Gao S 2016 A stable pentagonal bipyramidal Dy(III) single-ion magnet with a record magnetization reversal barrier over 1000 K *J. Am. Chem. Soc.* **138** 5441
13. Harriman K L, Brosmer J L, Ungur L, Diaconescu P L and Murugesu M 2017 Pursuit of record breaking energy barriers: a study of magnetic axiality in diamide ligated DyIII single-molecule magnets *J. Am. Chem. Soc.* **139** 1420
14. Ding Y S, Chilton N F, Winpenny R E and Zheng Y Z 2016 On approaching the limit of molecular magnetic anisotropy: a near-perfect pentagonal bipyramidal dysprosium(III) single-molecule magnet *Angew. Chem. Int. Ed.* **55** 16071
15. Liu J-L, Chen Y-C and Tong M-L 2018 Symmetry strategies for high performance lanthanide-based single-molecule magnets *Chem. Soc. Rev.* **47** 2431
16. Surbella R G, Ducati L C, Autschbach J, Pellegrini K L, McNamara B K, Schwantes J M and Cahill C L 2018 Plutonium chlorido nitrato complexes: ligand competition and computational metrics for assembly and bonding *Chem. Commun.* **54** 12014
17. Gaggioli C A and Gagliardi L 2018 Theoretical investigation of plutonium-based single-molecule magnets *Inorg. Chem.* **57** 8098
18. Antunes M A, Pereira L C, Santos I C, Mazzanti M, Marcalo J and Almeida M 2011 [U(TpMe2)2(bipy)]+:

A Cationic Uranium(III) Complex with Single-Molecule-Magnet Behavior *Inorg. Chem.* **50** 9915
19. Coutinho J T, Antunes M A, Pereira L C, Marcalo J and Almeida M 2014 Zero-field slow magnetic relaxation in a uranium(III) complex with a radical ligand *Chem. Commun.* **50** 10262
20. Pereira L C, Camp C, Coutinho J T, Chatelain L, Maldivi P, Almeida M and Mazzanti M 2014 Single-molecule-magnet behavior in mononuclear homoleptic tetrahedral Uranium(III) complexes *Inorg. Chem.* **53** 11809
21. Rinehart J D, Meihaus K R and Long J R 2010 Observation of a secondary slow relaxation process for the field-induced single-molecule magnet U(H2BPz2)3 *J. Am. Chem. Soc.* **132** 7572
22. Rinehart J D and Long J R 2009 Slow magnetic relaxation in a trigonal prismatic uranium(III) complex *J. Am. Chem. Soc.* **131** 12558
23. Layfield R, Guo F S, Mansikkamaki A, Tong M L and Chen Y C 2019 Uranocenium: synthesis, structure, and chemical bonding *Angew. Chem. Int. Ed. Engl.* 10.1002/anie.201903681
24. Coutinho J T, Antunes M A, Pereira L C, Bolvin H, Marçalo J, Mazzanti M and Almeida M 2012 Single-ion magnet behaviour in [U (Tp Me2) 2 I] *Dalton Trans.* **41** 13568
25. Chatelain L, Pécaut J, Tuna F and Mazzanti M 2015 Heterometallic Fe2II–UV and Ni2II–UV Exchange-Coupled Single-Molecule Magnets: Effect of the 3 d Ion on the Magnetic Properties *Chem. Eur. J.* **21** 18038
26. Chatelain L, Tuna F, Pécaut J and Mazzanti M 2015 A zig-zag uranyl(v)–Mn(ii) single chain magnet with a high relaxation barrier *Chem. Commun.* **51** 11309
27. Dey S, Velmurugan G and Rajaraman G 2019 How important is the coordinating atom in controlling magnetic anisotropy in uranium (iii) single-ion magnets? A theoretical perspective *Dalton Trans.* **48** 8976
28. Jung J, Atanasov M and Neese F 2017 Ab initio ligand-field theory analysis and covalency trends in actinide and lanthanide free ions and octahedral complexes *Inorg. Chem.* **56** 8802
29. Rinehart J D and Long J R 2012 Slow magnetic relaxation in homoleptic trispyrazolylborate complexes of neodymium(iii) and uranium(iii) *Dalton Trans.* **41** 13572
30. Le Roy J J, Gorelsky S I, Korobkov I and Murugesu M 2015 Slow magnetic relaxation in Uranium(III) and Neodymium(III) cyclooctatetraenyl complexes *Organometallics* **34** 1415
31. Meihaus K R, Minasian S G, Lukens W W Jr, Kozimor S A, Shuh D K, Tyliszczak T and Long J R 2014 Influence of pyrazolate vs N-heterocyclic carbene ligands on the slow magnetic relaxation of homoleptic trischelate lanthanide(III) and uranium(III) complexes *J. Am. Chem. Soc.* **136** 6056
32. van Leusen J, Speldrich M and Kögerler P 2018 Magnetism of actinide coordination compounds https://doi.org/10.1007/3418_2018_7
33. Singh M K, Yadav N and Rajaraman G 2015 Record high magnetic exchange and magnetization blockade in $Ln_2@C_{79}N$ (Ln = Gd(III) and Dy(III)) Molecules: A theoretical perspective *Chem. Commun.* **51** 17732
34. Singh M K and Rajaraman G 2016 Acquiring a record barrier height for magnetization reversal in lanthanide encapsulated fullerene molecules using DFT and ab initio calculations *Chem. Commun.* **52** 14047
35. Chen Y-C, Liu J-L, Ungur L, Liu J, Li Q-W, Wang L-F, Ni Z-P, Chibotaru L F, Chen X-M and Tong M-L 2016 Symmetry-supported magnetic blocking at 20 K in pentagonal bipyramidal Dy(III) single-ion magnets *J. Am. Chem. Soc.* **138** 2829
36. Gregson M, Chilton N F, Ariciu A-M, Tuna F, Crowe I F, Lewis W, Blake A J, Collison D, McInnes E J and Winpenny R E 2016 A monometallic lanthanide bis(methanediide) single molecule magnet with a large energy barrier and complex spin relaxation behaviour *Chem. Sci.* **7** 155
37. McClain K R, Gould C A, Chakarawet K, Teat S J, Groshens T J, Long J R and Harvey B G 2018 High-temperature magnetic blocking and magneto-structural correlations in a series of dysprosium(iii) metallocenium single-molecule magnets *Chem. Sci.* **9** 8492
38. Hänninen M M, Mota A J, Sillanpää R, Dey S, Velmurugan G, Rajaraman G and Colacio E 2018 Magneto-structural properties and theoretical studies of a family of simple heterodinuclear Phenoxide/Alkoxide bridged MnIIILnIII complexes: on the nature of the magnetic exchange and magnetic anisotropy *Inorg. Chem.* **57** 3683
39. Gupta S K, Rajeshkumar T, Rajaraman G and Murugavel R 2016 An unprecedented zero field neodymium(iii) single-ion magnet based on a phosphonic diamide *Chem. Commun.* **52** 7168
40. Chibotaru L F and Ungur L 2012 Ab initio calculation of anisotropic magnetic properties of complexes. I. Unique definition of pseudospin Hamiltonians and their derivation *J. Chem. Phys.* **137** 064112
41. Rudowicz C 1985 Transformation relations for the conventional O_k^q and normalised $O'_k{}^q$ Stevens operator equivalents with $k = 1$ to 6 and $-k \leq q \leq k$ *J. Phys. C Solid State Phys.* **18** 1415
42. Baldoví J J, Clemente-Juan J M, Coronado E, Duan Y, Gaita-Ariño A and Giménez-Saiz C 2014 Construction of a general library for the rational design of nanomagnets and spin qubits based on mononuclear f-block complexes. The polyoxometalate case *Inorg. Chem.* **53** 9976
43. Arauzo A, Lazarescu A, Shova S, Bartolomé E, Cases R, Luzón J, Bartolomé J and Turta C 2014 Structural and magnetic properties of some lanthanide (Ln = Eu(iii), Gd(iii) and Nd(iii)) cyanoacetate polymers: field-induced slow magnetic relaxation in the Gd and Nd substitutions *Dalton Trans.* **43** 12342
44. Jassal A K, Aliaga-Alcalde N, Corbella M, Aravena D, Ruiz E and Hundal G 2015 Neodymium 1D systems: targeting new sources for field-induced slow magnetization relaxation *Dalton Trans.* **44** 15774